Giant Relaxation Oscillations in a Very Strongly Hysteretic SQUID ring-Tank Circuit System

T.D. Clark,* R.J. Prance, R. Whiteman, H. Prance, and M.J. Everitt
Quantum Circuits Group, School of Engineering,
University of Sussex, Brighton, Sussex BN1 9QT, U.K.

A.R. Bulsara
Space and Naval Warfare Systems Centre, San Diego, CA 92152-5001, USA.

J.F. Ralph
Department of Electrical Engineering and Electronics,
Liverpool University, Brownlow Hill, Liverpool, L69 3GJ, UK.

In this paper we show that the radio frequency (rf) dynamical characteristics of a very strongly hysteretic SQUID ring, coupled to an rf tank circuit resonator, display relaxation oscillations. We demonstrate that the the overall form of these characteristics, together with the relaxation oscillations, can be modelled accurately by solving the quasi-classical non-linear equations of motion for the system. We suggest that in these very strongly hysteretic regimes SQUID ring-resonator systems may find application in novel logic and memory devices.

PACS numbers: 85.25.Dq, 74.50. + r

I. INTRODUCTION

Over the years the non-linear, dynamical properties of SQUID rings (i.e. thick superconducting rings containing either one or two Josephson weak link devices) have formed the basis of a range of technologically important devices [1], most recently through the phenomenon of stochastic resonance [2]. Apart from these applications, the study of the physics of the SQUID rings themselves [1, 3, 4, 5] has added considerably to the general field of non-linear dynamics. As studied previously, these dynamical properties have been due to the quasi-classical behaviour of SQUID rings in the regime where quantum processes can be neglected. However, of late much interest has been shown in the use of SQUID rings as purely quantum devices in possible quantum technologies [6]. This interest has been encouraged by recent experimental work on superposition states in weak link circuits [7, 8, 9, 10, 11, 12, 13] and, in particular, on SQUID rings [14, 15]. Inevitably, at some stage, quantum circuits are required to interact with classical probe circuits if information about their quantum state/evolution is to be extracted. As we have shown, for the case of the SQUID ring this interaction leads to the growth of non-linear behaviour in the classical part of the system [5, 16, 17, 18]. Thus, from this perspective, non-linear dynamics always has a crucial role to play in the description, quantum or quasi-classical, of SQUID rings. In this paper we shall demonstrate that, even with the quite understandable attention being paid to SQUID rings at the quantum level, there is much still to be explored in the quasi-classical regime. This can add greatly to our knowledge of non-linear systems and could lead to novel and powerful applications.

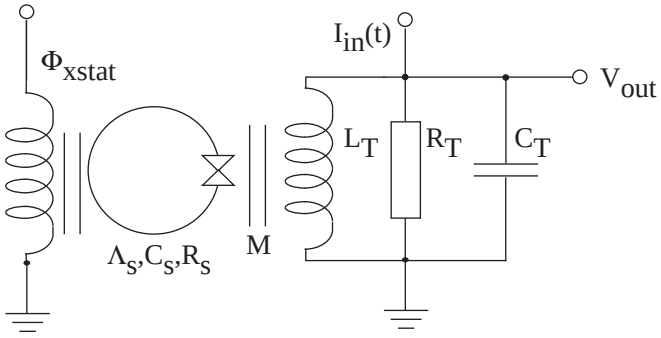

FIG. 1: Schematic of the coupled SQUID ring-rf tank circuit system also showing the static magnetic flux bias Φ_{xstat} applied to the ring.

In the description of SQUID rings [1] it is customary (from this quasi-classical viewpoint) to identify regimes of behaviour in terms of the parameter $\beta\,(=2\pi\Lambda I_c/\Phi_0)$, where Λ_s is the ring inductance, I_c is the (Josephson) critical current of the weak link in the ring and $\Phi_0 = h/2e$. In the presence of an external magnetic flux Φ_x the response of a SQUID ring is to set up a screening supercurrent $I_s\,(\Phi_x)$. The functional form of $I_s\,(\Phi_x)$ depends on the value of β. Thus, for $\beta \leq 1$, I_s is always single valued in Φ_x while for $\beta > 1$ this current is multi-valued and hysteretic in Φ_x. In this latter regime $I_s\,(\Phi_x)$ can be viewed as a set of approximately diamagnetic branches with switching between adjacent branches (in the absence of noise) occurring when I_s reaches $\pm I_c$. Given this branch switching, hysteresis loops will be swept out, with concomitant dissipation, when I_s exceeds $\pm I_c$. Devices

*Electronic address: t.d.clark@sussex.ac.uk

which utilize the properties of single weak link SQUID rings, such as magnetometers [1], are usually operated at low β values (e.g. 2 to 5). In operation as magnetometers single weak link SQUID rings are typically coupled inductively to a radio frequency (rf $\approx$ 20MHz), parallel LC, tank circuit which is excited using an rf current source. This arrangement is shown schematically in figure 1. As is well known, the rf voltage developed across the tank circuit is a function of both the rf magnetic flux amplitude and the static magnetic flux (Φ_{xstat}) applied to the ring. This static flux dependence is periodic in Φ_0, hence the use of the SQUID ring-tank circuit system in magnetometry.

The dynamical behaviour of a SQUID ring coupled to an external resonant circuit is governed, ultimately, by the form of its potential $U(\Phi, \Phi_x)$. Quasi-classically [1] (i.e. when the effective mass of the ring - the weak link capacitance C - is large, typically 10^{-12} to 10^{-14}F for 4 Kelvin operation) this potential has the form

$$U(\Phi, \Phi_x) = \frac{(\Phi - \Phi_x)^2}{2\Lambda_s} - \left(\frac{I_c \Phi_0}{2\pi}\right) \cos\left(\frac{2\pi\Phi}{\Phi_0}\right) \qquad (1)$$

where $\Phi\,(= \Phi_x + \Lambda I_s)$ is the total included flux in the ring. Clearly, if Φ_x changes slowly with time (i.e. slowly compared with any ring time constants), the ring will always remain at, or very close to, the minimum in $U(\Phi, \Phi_x)$. In dealing with ring-resonator dynamics it has been customary to assume that this adiabatic constraint is satisfied, e.g. in the low β rf SQUID magnetometer where the peak rf flux at the ring typically $\gtrsim \Phi_0$ ($= \mu\varphi$ for a fraction μ of the tank circuit flux φ coupled to the ring). The current I_s set up in response to this flux then couples back to the tank circuit, and so on. This back reaction, which reflects $I_s(\Phi_x)$, affects the rf voltage V_{out} of the tank circuit in a non-linear way. With I_{in} linearly amplitude modulated in time (e.g. at $\approx$ 100Hz), the result is the rf SQUID magnetometer (V_{out} verses I_{in}) characteristics. Following an initial linear riser in V_{out} versus I_{in}, these characteristics consist of a set of voltage plateaux (steps) spaced at regular intervals along I_{in}, with period $\propto \Phi_0/\Lambda$. The Φ_0-periodic modulation of these step features by a static (or quasi-static) applied flux Φ_{xstat} forms the basis of the rf SQUID magnetometer.

In this paper we report on the experimental and theoretical investigation of single weak link SQUID rings in the so-termed very strongly hysteretic regime, a previously little explored part of the parameter space of SQUID behaviour. With the SQUID ring inductively coupled to a high quality factor (Q) radio frequency ($rf \approx$ 20MHz) resonant circuit, we show that quite remarkable non-linear phenomena (large amplitude relaxation oscillations) can develop. We demonstrate that exactly these dynamics are solutions of the coupled non-linear equations of motion of the system.

II. SQUID RING-TANK CIRCUIT DYNAMICS IN THE STRONGLY HYSTERETIC REGIME

A. Quasi-classical equations of motion

The quasi-classical description of the ring-tank circuit system is based on the resistively shunted junction plus capacitance (RSJ+C) model of a weak link. Here, the supercurrent channel through the link is in parallel with a normal current channel (resistance R_s) and a capacitance C_s. In the model the normal channel turns on when the link current $I > I_c$. With representative values of C_s from 10^{-12} to 10^{-13}F, generally accepted resistances R_s are in the 10 to 100Ω range [19]. With this in mind, the coupled ring-tank circuit equations of motion are [1, 20]

$$\text{SQUID ring}: C_s\frac{d^2\Phi}{dt^2} + \frac{1}{R_s}\frac{d\Phi}{dt} + I_c \sin\left(\frac{2\pi\Phi}{\Phi_0}\right) + \frac{\Phi}{\Lambda_s(1-K^2)} = \frac{\mu\varphi}{\Lambda_s(1-K^2)} \qquad (2)$$

$$\text{Tank circuit}: C_T\frac{d^2\varphi}{dt^2} + \frac{1}{R_T}\frac{d\varphi}{dt} + \frac{\varphi}{L_T(1-K^2)} = I_{in}(t) + \frac{\mu\Phi}{\Lambda_s(1-K^2)} \qquad (3)$$

for tank circuit capacitance, inductance and parallel resonance resistance C_T, L_T and R_T, respectively, coupling constant $K = \sqrt{M^2/L_T\Lambda}$ for mutual inductance M, and Josephson current $I = I_c \sin(2\pi\Phi/\Phi_0)$. It is apparent in (2) that there are several possible ring time constants $\left(C_sR_s, \Lambda_s/Rs, 1/\sqrt{\Lambda_s C_s}\right)$. Clearly, if the adiabatic constraint holds, and there are no time constant problems, the derivative terms in (2) can be neglected and (2) reduces to

$$I_c \sin(2\pi\Phi/\Phi_0) + \Phi/\Lambda_s\left(1-K^2\right) = \mu\varphi/\Lambda_s\left(1-K^2\right) \qquad (4)$$

In the past this, together with (2), has been the starting point of most dynamical descriptions of ring-tank circuit systems, at least for low β SQUID rings. We note that in this linearized, small β, description I_c (i.e. β) can be found from the point of onset in I_{in} of the periodic step features in V_{out} versus I_{in} (the breakpoint) beyond the

initial linear riser [21].

As we emphasized recently [20], the adiabatic constraint breaks down when the ring is strongly hysteretic and underdamped [22]. Qualitatively, at 4 Kelvin, transition widths for branch switchings in I_s (Φ_x) are typically $\approx \Phi_0/100$. At 20MHz, and at the rf drive levels used experimentally for a $\beta \approx 50 - 100$ ring ($\mu\varphi \gtrsim 100\Phi_0$), the available time to switch between branches $\approx 10^{-12}$secs, comparable to the shortest ring time constant. In this range of β novel multiple level structures develop in the experimental V_{out} versus I_{in} characteristics [20]. These structures (plateaux of almost constant V_{out} along I_{in}) are on a scale in I_{in} large compared with standard rf SQUID magnetometer steps. However, these still maintain a form of Φ_0-periodicity in Φ_{xstat}. We also demonstrated numerically that these multiple level structure characteristics formed a new and particular class of solutions of (2) and (3). Given the range of non-linear phenomena that have already been recognized in ring-tank circuit systems, it would be surprising if these multiple level structures constituted the only new class of solutions in the high β regime. At even higher β a second type of non-linear dynamics (also a solution of 2 and (3) develops - relaxation oscillations in rf voltage against current - on scales very large ($\approx \times 10$) compared with conventional SQUID magnetometer characteristics.

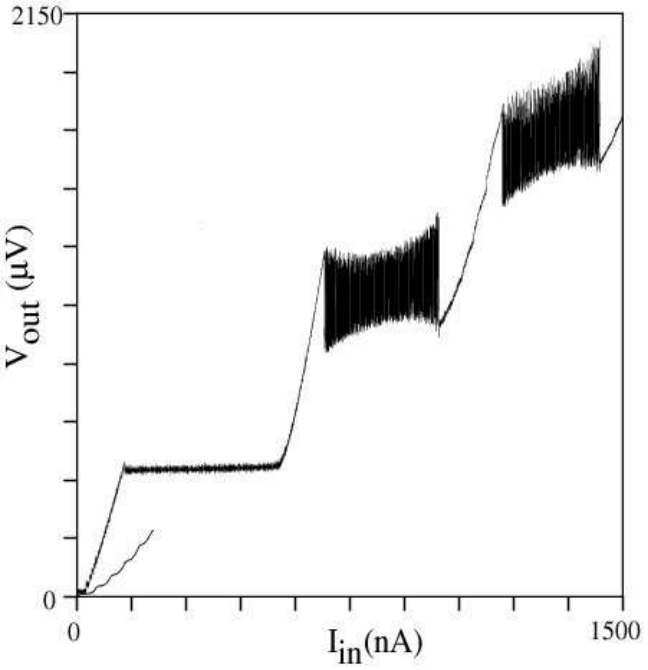

FIG. 2: Experimental (4.2 Kelvin, $\Phi_{\rm xstat} = n\Phi_{\rm o}$, $\Lambda = 6 \times 10^{-10}$H, $L_{\rm t} = 6.3 \times 10^{-8}$H, $f_{\rm rf} = 22.671$MHz, $K^2 = 0.008$ and $Q = 515$) $V_{\rm out}$ versus $I_{\rm in}$ characteristic for a niobium point contact SQUID ring-rf tank circuit system in the very highly hysteretic regime showing large scale relaxation oscillations. Here, the triangular ramp amplitude modulation of the rf is at 18Hz and the detection bandwidth of the receiver is 1MHz.

B. Experimental $V_{\rm out}$ versus $I_{\rm in}$ characteristics

In our experiments we made use of Zimmerman, 2-hole, niobium point contact SQUID rings [23]. The point contact weak links in these rings were adjusted, in situ, at liquid helium temperatures [17, 20], a technique which allows us to make weak links in a controlled way over a very wide range of β values (e.g. $1 < \beta < 100$). In our experimental arrangement the tank circuit voltage V_{out} (figure 1) was first amplified by a liquid helium cooled GaAsFET preamplifier (gain $\simeq$ 20dB, noise temperature < 10 Kelvin). This signal was further boosted using a receiver of our own design and then diode detected. Overall, the receiver system (including the GaAsFET preamplifier) was designed to combine very low noise with very large dynamic range and slew rate, all three properties being required to observe the very strongly hysteretic behaviour reported here.

In figure 2 we show a perfectly typical experimental diode detected V_{out} versus I_{in} SQUID magnetometer characteristic in this very strongly hysteretic regime. This was taken at 4.2 Kelvin, in a bandwidth of 1MHz, with $Q = 515$, $K^2 = 0.008$ and a static bias flux $\Phi_{xstat} = n\Phi_0$, n integer, supplied by a second coil coupled to the ring (figure 1). Here, adopting common practice, this characteristic was recorded at the $n\Phi_{\rm o}$ bias frequency f_{rf} (22.671MHz in this case) equal to the resonant frequency of the ring-tank circuit system when $\Phi_{xstat} = n\Phi_0$. As is standard for these dynamical (SQUID magnetometer) characteristics, the rf is amplitude modulated using a low frequency triangular ramp. In this example the ramp frequency is 18Hz. As can be seen, the characteristic consists of a first feature, a flat step, followed by two further step features in which it is apparent that V_{out} oscillates very rapidly as I_{in} increases. Although not shown in figure 2, these oscillatory step structures, periodic in I_{in}, continued to repeat as I_{in} was made larger. The rf voltage and current scales in figure 2 are made clear by the small, subsidiary characteristic in the same figure. This was taken at 4.2 Kelvin, with $\Phi_{xstat} = n\Phi_0$, using the SQUID ring and tank circuit of the main characteristic but with the weak link in the ring adjusted to give a β just greater than unity, i.e. the regular rf SQUID magnetometer regime. It is obvious that the scalings of the main characteristic are very large indeed compared to those for a standard SQUID magnetometer. In figure 3 we show details of the second step structure of figure 2 along which the large scale oscillations first appear. Here, we have expanded the first section of this step structure (shown boxed in figure 3). In the expanded picture it is apparent that V_{out} is undergoing rapid oscillations as I_{in} is increased. Furthermore, the spacing in I_{in} between adjacent oscillations decreases monotonically as I_{in} is swept across the step; this continues right across the step (not shown in figure 3). We note that the effect of a bias flux Φ_{xstat} on these oscillatory step structures was minimal, only changing the amplitude of

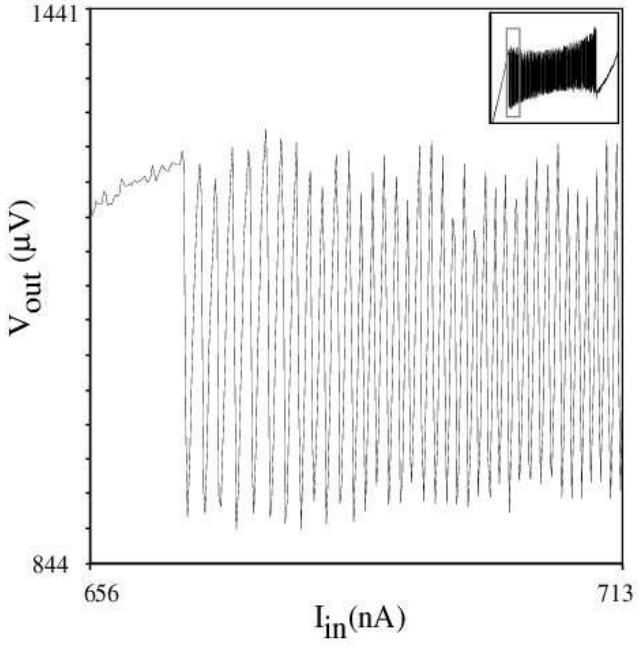

FIG. 3: Expanded region of the second plateau in figure 2 showing details of the relaxation oscillations.

the oscillations very weakly, with a periodicity of Φ_0. Experimentally, a search of the first (flat) step in figure 1 did not reveal any voltage oscillations, only noise. Again, the effect of Φ_{xstat} was found to be negligible.

The waveform of figure 3 reflects a limit cycle consisting of a very slow build up (at least on the time scale of one rf oscillation $2\pi/\omega_{rf}$) followed by an extremely fast discharge with energy drawn from the tank circuit. This is the followed by the next slow build up with energy supplied from the rf current source over many rf periods, and so on.These are, of course, relaxation oscillations which can be found in many physical situations where non-linear dynamics is involved [28, 29, 30, 31]. For the particular case of the driven SQUID ring-tank circuit system of figure 3, the peak rf amplitude is increasing (linearly ramped with time) from left to right. Since the energy is made up from the rf current drive, this means that the time interval between successive oscillations shortens as I_{in} increases, as is apparent in figure 3.

Without the combination of very low noise receiver (including a liquid helium cooled GaAsFET preamplifier stage) and very large dynamic range/slew rate capability, the relaxation oscillations shown in figures 2 and 3 would not be observed. For example, reduced bandwidth or added noise, or a combination of both, can wash out these oscillations. What then remain are large (compared with ordinary SQUID magnetometer characteristics - see insert figure 2), roughly constant rf voltage, current steps. This is presumably why these dynamics have not been observed in the past.

It is interesting to note that the relaxation oscillations observed by us in coupled SQUID ring-tank circuit systems in the very strongly hysteretic regime appear to have analogues in the phase slippage experiments which have been performed on superfluid helium systems [25, 26, 27]. It seems clear that, putting the fundamental description of superfluid and superconducting condensates aside, the phase/flux slippage in the two systems is analogous. At a phenomenological level this means that the equations of motion governing the dynamics of the two ring-resonator systems are also analogous. In the highly hysteretic regime for phase slippage in superfluid rings containing weak link orifices we would therefore expect to see (giant) relaxation oscillation phenomena and, perhaps, multilevel dynamics [20].

C. Numerical calculations

The $V_{\rm out}$ versus $I_{\rm in}$ characteristics of figures 1 and 2 can be modelled using (2) and (3) which can handle the problem of non-adiabaticity perfectly well [20]. However, since for typical SQUID ring parameters ($C_s \approx 10^{-13}$F, $\Lambda_s = 6 \times 10^{-10}$H, $R_s \approx 10\Omega$), the ring time constants will be 2 or more orders of magnitude shorter than the tank circuit time constant ($\cong 1/20$MHz), great care must be taken to ensure that accurate solutions are found. To solve (2) and (3) we used fourth order Runge-Kutta with an adaptive step size algorithm [5, 17, 20]. We were also careful allow a sufficient number of steps per rf cycle to follow the changes in the SQUID ring accurately. For our comparison with experiment we set the rf drive frequency at the $\Phi_{xstat} = n\Phi_0$ resonant frequency (the pseudoresonant frequency [5, 17, 20]). At this bias flux the ring is at its most diamagnetic [with a ring magnetic susceptibility $\chi\left(n\Phi_0\right) = \partial I_s\left(n\Phi_0\right)/\partial\Phi_x \cong -1$] and I_s is almost linear in Φ_x. From the data of figure 2 we can make an estimate of I_c (and hence β) from the start of the step features in the standard SQUID magnetometer compared with the (first) step feature in the large scale characteristics [20]. This yields an I_c for the large β characteristic $\cong 80\mu$A (i.e. a β value in the 70 to 80 range). We have shown [24] that knowing I_c and the Fermi velocity of the material of the SQUID ring (here niobium) we can estimate C. For $I_c \simeq 100\mu$A this gives $C_s \approx$ few$\times 10^{-13}$F. In addition, from singly connected current-voltage characteristics for point contact weak links[19], a typical value for R_s at this I_c is $\approx 10\Omega$.

In figure 4 we show the results of solving (2) and (3) to simulate the behaviour of the ring-tank circuit system of figures 2 and 3, including a 4 Kelvin noise source [5, 17, 20]. Given the very non-linear nature of this coupled system, and the number of parameters involved, an exact match between theory and experiment has proved difficult. Nevertheless, we were able to reproduce the important features of the integer bias flux V_{out} versus I_{in} characteristic of figures 2 and 3 with $I_c = 80\mu$A and best fit values $C_s = 5 \times 10^{-13}$F, $R_s = 10\Omega$ and $f_{rf} = 25$MHz. The other circuit parameters are, as for figures 2 and 3, $Q = 515$, $K^2 = 0.008$, $L_T = 63n$H,

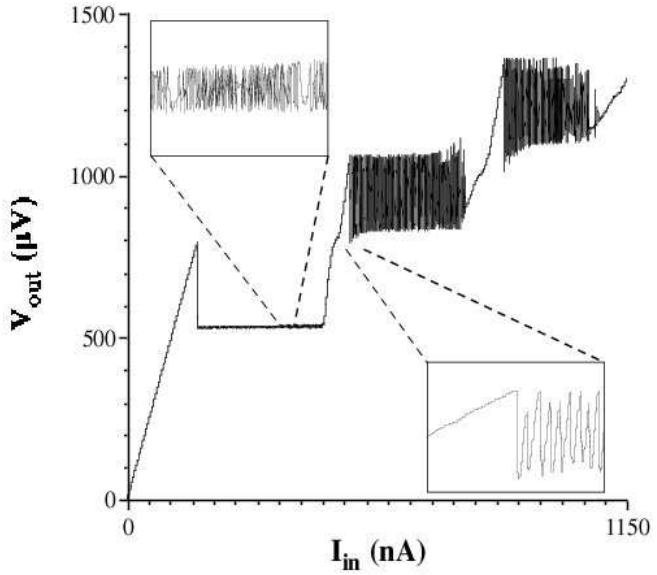

FIG. 4: Theoretical (RSJ+C) $V_{\rm out}$ versus $I_{\rm in}$ characteristic (with a 4 Kelvin tank circuit noise source added) to model the data of figures 2 and 3, setting $\Phi_{\rm xstat} = n\Phi_{\rm o}$, $\Lambda_{\rm s} = 6\times10^{-10}$H, $L_{\rm t} = 6.3 \times 10^{-8}$H, $K^2 = 0.008$, $Q = 515$ and a best fit $f_{\rm rf} = 25$MHz. Here, the effective triangular ramp amplitude modulation frequency is close to 30Hz.

while the effective triangular ramp frequency (converted from an rf current ramp in μA/sec) is close to 30Hz. As can be seen, the computed solution contains both the first flat step and the relaxation oscillations on the second (and subsequent) step features of figure 2. Details of these (computed) oscillations are shown in the lower inset in figure 4. Also shown inset, over a small range of $I_{\rm in}$ in the same figure, is a highly expanded section of the first flat step. This too displays (weak) voltage oscillations which appear to be either aperiodic or multiperiodic. These oscillations were not seen experimentally, presumably because of limited signal to noise. If I_{in} is fixed in the regions corresponding to the insets in figure 4 - for the experimental data set of figure 2, and time series data are collected, these weak oscillations can be seen reflected in the (pseudo) phase portrait, as shown in figure 5(a). Here, the pseudo-phase portrait is defined as a plot of $V_{out}\,(t)$ against the time shifted $V_{out}\,(t+\tau)$ at all times t, where τ is a suitable time delay $\left(10^{-4}\,\text{sec}\,\text{in this example}\right)$. In the main part of figure 5(a) we show the pseudo phase portrait, taken over a set of complete orbits, for the bias point in the upper inset. In the lower inset we display just one of these orbits. It is clear, for the first step, that this pseudo-phase portrait simply shows random fluctuations (noise) superimposed on a singly periodic orbit. This should be contrasted with the pseudo-phase portrait of figure 5(b) for I_{in} biased onto the middle of the relaxation oscillations in the second V_{out} versus I_{in} step feature [shown in the upper inset of figure 5(b)]. Here, we have again plotted a set of orbits, with a single orbit of this set shown in

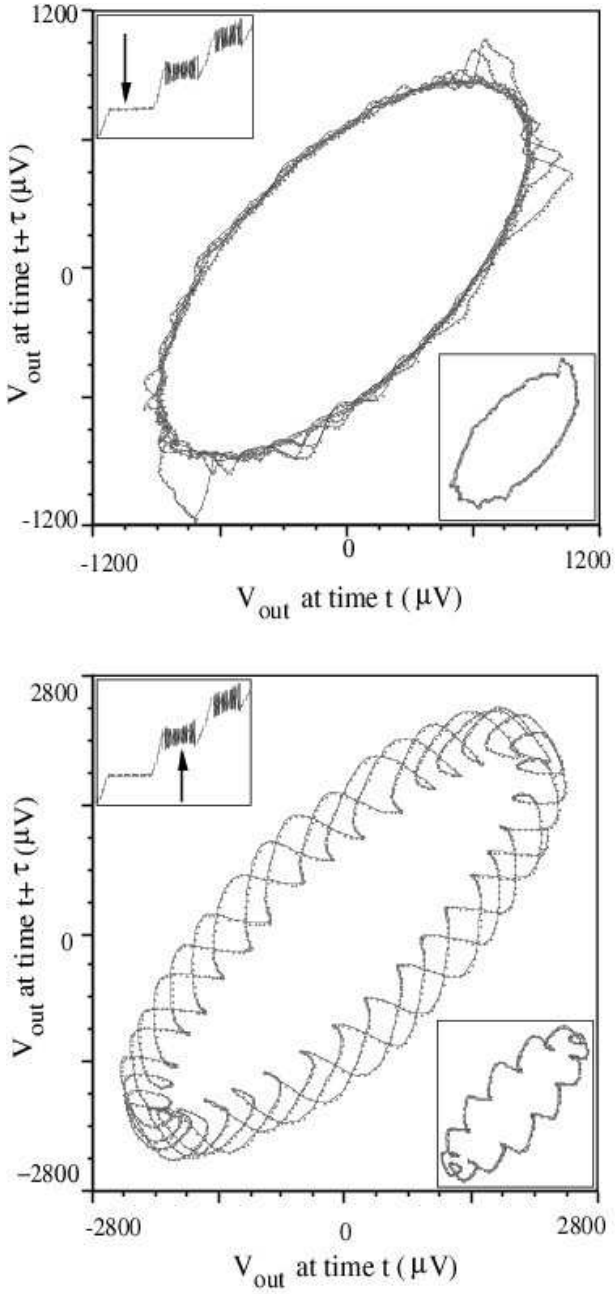

FIG. 5: Experimental pseudo phase portraits ($V_{\rm out}\,(t+\tau)$, taken over sets of complete orbits, versus $V\,(t)$) for the two $I_{\rm in}$ bias points of figure 2 as shown arrowed in the insets. Here, $\tau = 10^{-4}\,\text{sec}$ and $T = 4.2$Kelvin. The lower insets in (a) and (b) display single orbits of the data sets for the two bias points. The data was obtained in a detection bandwidth of 1MHz with an 18Hz sweep frequency.

the lower inset. As is apparent both the set and the single orbit display the periodic behaviour associated with the relaxation oscillations on the step.

What the theoretical computations of figure 4, the experimental data of figures 2 and 3, and the previously published multilevel structures [20], demonstrate is that

the form of the solutions to the coupled equations of motion (2) and (3) is critically dependent on parameter values. More specifically, it appears that in the very strongly hysteretic regime and above (i.e. $\beta \gtrsim 100$) the underdamping in the ring-tank circuit system becomes sufficiently large to wash out multilevel structures completely, or almost completely. Physically, these structures arise (with stochastic jumping) from the system moving around n hysteresis loops in Φ versus Φ_x (or I_s versus Φ_x) in m rf cycles, n and m integer [22]. When sufficiently underdamped we assume that the system simply jumps between much larger values of Φ in Φ versus Φ_x, followed by long recovery period over many rf cycles, i.e. a relaxation oscillation process.

III. CONCLUSIONS

The experimental data of figures 2 and 3 are typical of the V_{out} versus I_{in} characteristics found in the very strongly hysteretic, and underdamped, regime ($\beta > 100$). These data can be modelled with considerable accuracy invoking the SQUID potential (1) and using the quasi-classical equations of motion (2) and (3), as can be seen from the computed V_{out} versus I_{in} characteristics of figure 4. Thus, from experiment and theory we find that there exists another class of solution, to the dynamics of the driven ring-tank circuit system in the very highly hysteretic regime, apart from multilevel structures [20]. Since these (latter) structures clearly hold out the real possibility of quasi-classical multilevel logic and memory if these dynamics are well understood and can be controlled, there is every reason for opening up the phase space of behaviour. Indeed, the potential for single flux quantum logic has already attracted a great deal of interest [32]. It seems reasonable, therefore, that multilevel logic based on the manipulation of sets of discrete flux states of a SQUID ring in the strongly hysteretic regime will also generate interest. From the work reported here, it would appear that the change over between multilevel and relaxation solutions is quite subtle and sensitive to circuit parameters. From experiment and theory we find that relaxation oscillation characteristics, very similar to those reported here, carry on to very much higher β values (> 500). This, of course, points to these being a rather general class of solutions to (2) and (3). Again, as with the earlier multilevel structures [20], these solutions do not arise in the linearized description of the system. We note, again from experiment and computation, that the multi-level structures [20] found in the strongly hysteretic regime with $\beta \approx 50$ gradually fade away as β increases, to be replaced by the relaxation oscillation characteristics reported in this paper. In our opinion, even though other factors may be important in governing the already underdamped dynamics of this highly non-linear system, this points to the damping becoming weaker as β grows. It also seems clear that a rich new field of non-linear dynamics exist which, as yet, has only been partially explored. From a historical perspective, it is also of interest that the original description of rf-biased SQUID magnetometers [21] was based on a relaxation oscillation model, albeit operating over very much shorter time intervals (a few rf periods), and on the rf voltage and current scales of conventional SQUID magnetometers [21]. Never the less, relaxation oscillations have not been seen in the dynamics of these standard magnetometers. To our best knowledge, the relaxation oscillations reported in this paper are the first to have been observed in the dynamical (V_{out} versus I_{in}) characteristics of SQUID ring-resonator systems on any scale or frequency.

IV. ACKNOWLEDGEMENTS

We would to express our thanks to the Engineering and Physical Sciences Research Council for its generous funding of this work.

[1] K.K. Likharev, "Dynamics of Josephson Junctions and Circuits" (Gordon and Breach, Sidney, 1986).
[2] See, for example, L. Gammaitoni, P. Hanggi, P. Jung, and F. Marchesoni, Rev. Mod. Phys. 70, 1 (1998); A.R. Bulsara, and L. Gammaitoni, Phys. Today 49, 39 (1996)
[3] A.R. Bulsara, J. Appl. Phys. 60, 2462 (1986).
[4] M.P. Soerensen, M. Barchelli, P.L. Christiansen, and A.R. Bishop, Phys. Lett. 109A, 347 (1985).
[5] T.D. Clark, J.F. Ralph, R.J. Prance, H. Prance, J. Diggins, and R. Whiteman, Phys. Rev. E 57, 4035 (1998)
[6] See, for example, H.K. Lo, S. Popescu and T.P. Spiller (Eds) "Introduction to Quantum Computation and Information", (World Scientific, New Jersey, 1998).
[7] T.P. Orlando, J.E. Mooij, L. Tian, C.H. van der Wal, L.S. Levitov, S. Lloyd and J.J. Mazo, Phys. Rev. B. 60, 15398 (1999).
[8] Y. Makhlin, G. Schön and A. Shnirman, Nature. 398, 305 (1999).
[9] D. Averin Nature 398, 748 (1999).
[10] R. Rouse, S. Han, J.E. Lukens, Phys. Rev. Lett. 75, 1614 (1995).
[11] P. Silvestrini, B.B. Ruggierio, C. Granata, E. Esposito, Phys. Lett. A 267, 45 (2000).
[12] Y. Nakamura, C.D. Chen, J.S. Tsai, Phys. Rev. Lett 79, 2328 (1997).
[13] Y. Nakamura, Y.A. Pashkin, J.S. Tsai, Nature 398, 786 (1999).
[14] C.H. van der Wal, A.C.J. ter Haar, F.K. Wilhem, R.N. Schouten, C.J.P.M. Harmans, T.P. Orlando, S. Lloyd, J.E. Mooij, Science 290, 773 (2000).
[15] J.R. Friedman, V. Patel, W. Chen, S.K. Tolpygo, J.E. Lukens, Nature 406, 43 (2000).
[16] J.F. Ralph, T.P. Spiller, T.D. Clark, R.J. Prance and

H. Prance, Int. J. Mod. Phys. B 8, 2637 (1994).
[17] R. Whiteman, J. Diggins, V. Schöllmann, T.D. Clark, R.J. Prance, H. Prance and J.F. Ralph, Phys. Letts. A 234, 205 (1997).
[18] R. Whiteman, V. Schöllmann, M.J. Everitt, T.D. Clark, R.J. Prance, H. Prance, J. Diggins, G. Buckling and J.F. Ralph, J. Phys.: Condens. Matter 10, 9951 (1998).
[19] J.E. Zimmerman, Proc. 1972 Applied Superconductivity Conference, Annapolis, 544-561 (IEEE Publications, New York, 1972).
[20] R.J. Prance, R. Whiteman, T.D. Clark, H. Prance, V. Schöllmann, J.F. Ralph, S. Al-Khawaja and M. Everitt, Phys. Rev. Letts. 82, 5401 (1999).
[21] O.V. Lounasmaa, "Experimental Principles and Methods below 1K" (Academic Press, London, 1974), pp. 156-159.
[22] E. Ben-Jacob and D. Abraham, Appl. Phys. Lett. 39, 835 (1981).
[23] J.E. Zimmerman, P. Thiene, and J.T. Harding, J. Appl. Phys. 41, 1572 (1970).
[24] J.F. Ralph, T.D. Clark, J. Diggins, R.J. Prance, H. Prance, and H. Prance, J.Phys. Condens. Matter 9, 8275 (1997).
[25] S.V. Pereverzev, A. Loshak, S. Backhaus, J.C. Davis and R.E. Packard, Nature 388, 449 (1997).
[26] K. Schwab, N. Bruckner and R.E. Packard, J. Low Temp. Phys. 110, 1043 (1998).
[27] E. Varoquaux, O. Avenal, G. Ihes and R. Salmelin, Physica B178, 309 (1992).
[28] S.H. Strogatz, "Non-linear Dynamics and Chaos" (Perseus Books, Reading, Mass., 1994), p.211.
[29] L.O. Chua, C.A. Desoer and E.S. Kuh, "Linear and Non-linear Circuits" (McGraw Hill, New York, 1987), p.344.
[30] J.M.T. Thompson and H.B. Stewart, "Non-linear Dynamics and Chaos" (John Wiley, Chichester, 1986), p.84.
[31] P. Glendinning, "Stability, Instability and Chaos"(Cambridge University Press, 1994), p.175.
[32] See V.P. Koshelets, K.K. Likharev and V.V. Migulin, IEEE T MAGN 23: (2) 755 (Mar. 1987); H. Miyake, N. Fukaya and Y. Okabe, IEEE T MAGN 21: (2) 578 (1985).